A Comparison between the Raman Spectra of Ce$_{1-x}$Ca$_x$VO$_{4-0.5x}$ (0 ≤ *x* ≤ 0.41) and Ce$_{1-x}$Bi$_x$VO$_4$ (0 ≤ *x* ≤ 0.68)

T. Hirata

National Research Institute for Metals, 1-2-1 Sengen, Tsukuba, Ibaraki 305-0047, Japan
E-mail: hirata@nrim.go.jp

and

A. Watanabe

National Institute for Research in Inorganic Materials, 1-1 Namiki, Tsukuba, Ibaraki 205-0044, Japan
E-mail: watanakt@nirim.go.jp

The Raman spectra of Ce$_{1-x}$Ca$_x$VO$_{4-0.5x}$ (0 ≤ *x* ≤ 0.41) and Ce$_{1-x}$Bi$_x$VO$_4$ (0 ≤ *x* ≤ 0.68) solid solutions, where aliovalent Ca^{2+} or isovalent Bi^{3+} cations are substituted for Ce^{3+} in the tetragonal cerium vanadate CeVO$_4$, are presented as a function of *x* to compare with each other. There was a remarkable difference in that the three broad features appeared in the Raman spectra of Ce$_{1-x}$Ca$_x$VO$_{4-0.5x}$ whereas they were absent for Ce$_{1-x}$Bi$_x$VO$_4$. The appearance of the broad features could be attributed to the "charge transfer" effect on the aliovalent Ca^{2+} substitution, which is responsible for a substantial enhancement in electrical conductivity in Ce$_{1-x}$Ca$_x$VO$_{4-0.5x}$ relative to Ce$_{1-x}$Bi$_x$VO$_4$ with *x*. From the changes in the modes' frequency with unit-cell volume, which exhibit a different decrease with *x* between Ce$_{1-x}$Ca$_x$VO$_{4-0.5x}$ and Ce$_{1-x}$Bi$_x$VO$_4$, we could estimate mode Grüneisen parameters that vary in magnitude and/or sign as well as between Ce$_{1-x}$Ca$_x$VO$_{4-0.5x}$ and Ce$_{1-x}$Bi$_x$VO$_4$; this reflects the fact that different lattice distortions are induced when aliovalent or isovalent cations with similar/different ionic radii are substituted to form both the solid solutions. © 2001 Academic Press

Key Words: Raman spectra; CeVO$_4$; Ce$_{1-x}$Ca$_x$VO$_{4-0.5x}$; Ce$_{1-x}$Bi$_x$VO$_4$; aliovalent or isovalent cation substitution; charge transfer; Grüneisen parameter.

INTRODUCTION

Recently Watanabe (1) found a remarkable increase in electrical conductivity in Ce$_{1-x}$M$_x$VO$_{4-0.5x}$ (*M* = Pb, Sr, and Ca) over that in Ce$_{1-x}$Bi$_x$VO$_4$ relative to the tetragonal cerium vanadate CeVO$_4$, which has space group D_{4h}^{49}–I4$_1$/amd (*Z* = 4) and lattice parameters *a* = 7.004 Å and *c* = 6.4977 Å (2–4). On the other hand, the solid solubility limit x_{max} and lattice parameters vary with *x*, i.e., *da/dx* or *dc/dx*, depending on the substitute, revealing that the valence and/or ionic radii of the substitutional atoms are crucial factors. Subsequently, T. Hirata and A. Watanabe (to be published) found some noticeable differences between the Raman spectra of Ce$_{1-x}$M$_x$VO$_{4-0.5x}$ and Ce$_{1-x}$Bi$_x$VO$_4$ as well as among *x*-varied solid solutions, encouraging us to do an in-depth study.

The present paper is concerned with a comparison between the Raman spectra of Ce$_{1-x}$Ca$_x$VO$_{4-0.5x}$ and Ce$_{1-x}$Bi$_x$VO$_4$, which are formed as aliovalent Ca^{2+} or isovalent Bi^{3+} cations are substituted for Ce^{3+} in CeVO$_4$, respectively. As evident from the lattice parameter changes with *x* shown in Fig. 1, Ce$_{1-x}$Ca$_x$VO$_{4-0.5x}$ exhibits $x_{max} \sim 0.41$ and relatively high values of *da(c)/dx*, whereas Ce$_{1-x}$Bi$_x$VO$_4$ reveals a large value of $x_{max} \sim 0.68$ but lower values of *da(c)/dx* as compared with Ce$_{1-x}$Ca$_x$VO$_{4-0.5x}$. The aliovalent Ca^{2+} (1.12 Å) has about the same ionic radius as Ce^{3+} (1.14 Å), and the radius of isovalent Bi^{3+} (1.17 Å) is also close to that of Ce^{3+} (5).

As far as we are concerned with Fig. 1, it is most likely that the different valences of Ca and Bi, as well as their slightly different ionic radii, could dominate the lattice parameter changes and/or the values of x_{max}. It is expected that aliovalent or isovalent cation substitution could cause Raman spectral changes of CeVO$_4$, motivating the present work. Here, it should be noted that the cerium valence in CeVO$_4$ is 3+, whereas the vanadium atom remains in the pentavalent state by X-ray absorption spectroscopy (6). Hence, a change of oxygen stoichiometry is induced to preserve charge neutrality for the aliovalent Ca substitution.
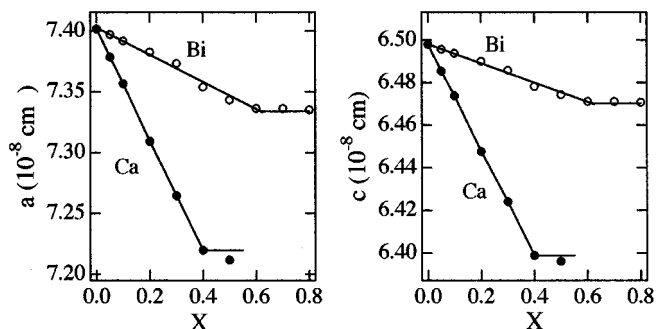
264

FIG. 1. Changes in the lattice parameters a and c with x for $Ce_{1-x}Ca_xVO_{4-0.5x}$ and $Ce_{1-x}Bi_xVO_4$, respectively.

EXPERIMENTAL

Substitutional solid solutions, $Ce_{1-x}Ca_xVO_{4-0.5x}$ and $Ce_{1-x}Bi_xVO_4$ with various x values, were prepared by a solid state reaction technique, whose details are given elsewhere (1). Raman scattering measurements were performed with pellets by a Dilor Raman spectrometer (Super Labram); the scattered light from the sample was collected with a CCD (Charge Coupled Device) detector. A 514.5-nm line from the Ar^+ laser was used as the radiation source. All the Raman spectra were measured in a back-scattering configuration at room temperature.

RESULTS AND DISCUSSION

Figure 2 depicts the Raman spectra of $Ce_{1-x}Ca_x VO_{4-0.5x}$ and $Ce_{1-x}Bi_xVO_4$ in the range 200–1000 cm^{-1}; the Raman spectrum of $CeVO_4$ is also shown, for reference. In the Raman spectrum of $CeVO_4$, which well agrees with the literature (7), five Raman modes are observed at 261, 372, 461, 771, and 847 cm^{-1}. The 372-, 461-, 771-, and 847-cm^{-1} Raman modes are assigned as $A_{1g} + B_{1g}$ deformation (ν_2), $E_g + B_{2g}$ deformation (ν_4), E_g asymmetric stretch (ν_3), and A_{1g} symmetric stretch (ν_1), respectively (7–9), while no assignment is made for the 261-cm^{-1} mode. We notice that the B_{2g} asymmetric stretch mode (ν_3) at 784 cm^{-1} accompanies the E_g symmetric stretch mode at 771 cm^{-1}, revealing the sign of two resolved peaks. Besides, a shoulder is apparent on the high-frequency side of the A_{1g} symmetric stretch mode at 847 cm^{-1}, and there is a small peak observed around 220 cm^{-1}, as detected in the literature (7).

Obviously, the observed Raman modes change systematically in frequency, linewidth, and intensity with increasing amounts of the substitutes for Ce in $CeVO_4$. Particularly, it is remarkable that the three broad features would emerge at approximately 495, 705, and 912 cm^{-1} and intensify with x for $Ce_{1-x}Ca_xVO_{4-0.5x}$, whereas they are absent in $Ce_{1-x}Bi_xVO_4$. With respect to the broad features appearing

only in $Ce_{1-x}Ca_xVO_{4-0.5x}$, the following arguments are possible.

In general, two effects on phonon properties of $CeVO_4$ are expected when aliovalent Ca^{2+} with a different ionic radius is substituted for Ce^{3+} to form $Ce_{1-x}Ca_xVO_{4-0.5x}$ (10–12). First, there is the "chemical pressure" effect induced by the variation in the average Ca/Ce ion size, which can somewhat explain the phonon frequency changes with the Ca substitution. However, this effect is not sufficient to account for the significant changes in phonon frequency and lattice parameters for $Ce_{1-x}Ca_xVO_{4-0.5x}$ with x. This is substantiated by the fact that the substitution of isovalent Bi^{3+} with an ionic radius similar to that of Ca^{2+} provides smaller phonon frequency/lattice parameter changes with x for $Ce_{1-x}Bi_xVO_4$ (T. Hirata and A. Watanabe, to be published). It is probable that the additional "charge transfer" effect induced by the aliovalent Ca^{2+} substitution could dominate the phonon properties and is responsible for the appearance of the three broad features in $Ce_{1-x}Ca_xVO_{4-0.5x}$. For the aliovalent Ca^{2+} substitution, the charge neutrality is preserved via a change in oxygen stoichiometry; the measured oxygen content supports the oxygen stoichiometric change on the Ca substitution in $Ce_{1-x}Ca_xVO_{4-0.5x}$ (1). The charge transfer effect also accounts for the pronounced enhancement in electrical conductivity in $Ce_{1-x}Ca_xVO_{4-0.5x}$ relative to $Ce_{1-x}Bi_xVO_4$ with no significant increase (1).

The oxygen stoichiometric change could affect the phonon properties of oxides, as is well-documented in high-T_c superconductors (13–15), which can lead to chemical/structural modifications. The chemical/structural differences can produce differing phonon density of states or
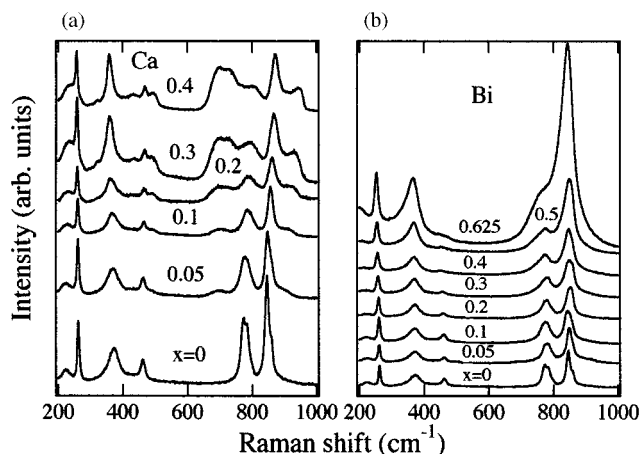

FIG. 2. The Raman spectra of $Ce_{1-x}Ca_xVO_{4-0.5x}$ and $Ce_{1-x}Bi_xVO_4$ in the range 200–1000 cm^{-1}; the Raman spectrum of $CeVO_4$ is also shown for reference. Note that each spectrum except for $CeVO_4$ is vertically shifted to avoid overlap. (a) $Ce_{1-x}Ca_xVO_{4-0.5x}$; $x = 0, 0.05, 0.1, 0.2, 0.3,$ and 0.4 (from bottom to top). (b) $Ce_{1-x}Bi_xVO_4$; $x = 0, 0.05, 0.1, 0.2, 0.3, 0.4, 0.5,$ and 0.625 (from bottom to top).
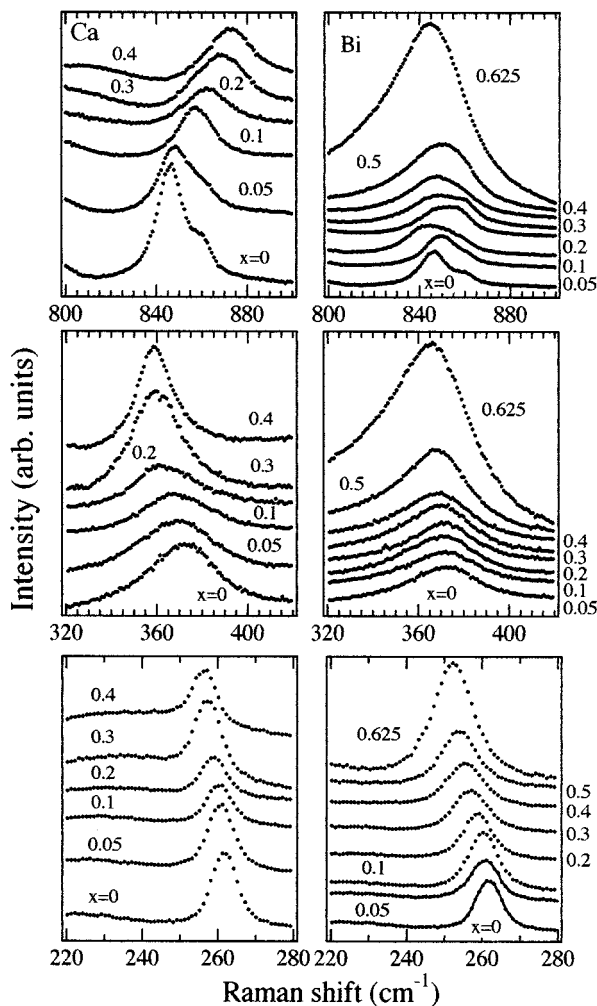
FIG. 3. The three Raman modes at 847, 372, and 261 cm^{-1} for Ce$_{1-x}$Ca$_x$VO$_{4-0.5x}$ and Ce$_{1-x}$Bi$_x$VO$_4$ with various x values, along with those for CeVO$_4$ for reference.

a disorder-induced broad band as observed in the Raman spectra of TiO$_2$ (16, 17), which could be associated with several distinctive/interesting spectral features between

Ce$_{1-x}$Ca$_x$VO$_{4-0.5x}$ and Ce$_{1-x}$Bi$_x$VO$_4$. A further investigation is requested in more detail.

In the present work, we pay attention to the three Raman modes at 847, 372, and 261 cm^{-1} for CeVO$_4$, which change in frequency, linewidth, and intensity with x as shown in Fig. 3. Interestingly, the A_{1g} symmetric stretch mode at 847 cm^{-1} shifts upward, whereas the $A_{1g} + B_{1g}$ deformation mode at 372 cm^{-1} and the 261-cm^{-1} mode shift downward with x. It is noticeable that the 847-cm^{-1} mode in Ce$_{1-x}$Bi$_x$VO$_4$ exhibits no significant frequency change, but rather tends to be stationary with x. The upward shift of the 847-cm^{-1} symmetric stretch mode with x is due to shortening of V–O lengths, and hence there is an increase in force constants, as evidenced by the lattice parameter decrease with x. Consequently, no remarkable frequency change of the mode for Ce$_{1-x}$Bi$_x$VO$_4$ relative to Ce$_{1-x}$Ca$_x$VO$_{4-0.5x}$ can be reconciled with the fact that the lattice parameter decrease with x is less significant in the former than in the latter (see Fig. 1). As for the other two modes, the force constants would decrease because of the distortion of VO$_4$ tetrahedra with the cation substitution, resulting in the downward shift of the modes with x.

Here, we show that the mode-dependent change in frequency must be reflected in the size and/or sign of the mode Grüneisen parameter. The mode Grüneisen parameter γ_i is defined by (18, 19)

$$\gamma_i = - \, d \ln \omega_i / d \ln V = - V / \omega_i (d\omega_i / dV), \qquad [1]$$

where ω_i is the ith mode frequency, and V the unit-cell volume. Equation [1] tells us that the mode Grüneisen parameter can be determined by plotting the mode frequency vs the unit-cell volume, as shown for Ce$_{1-x}$Ca$_x$VO$_{4-0.5x}$ and Ce$_{1-x}$Bi$_x$VO$_4$ in Fig. 4. We notice that the plots would be nonlinear rather than linear for the 847- and 372-cm^{-1} modes, while a linear correlation predominates for the 262-cm^{-1} mode. Approximately, the Grüneisen parameters of the 847- and 372-cm^{-1} modes are determined from the linear portion as drawn in Fig. 4. The
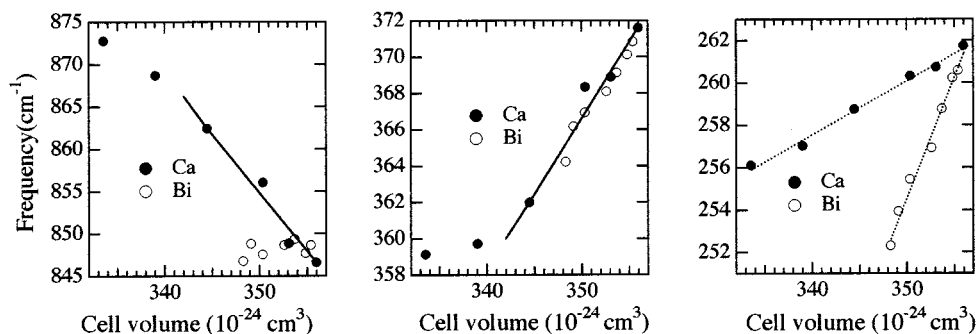

FIG. 4. The frequency changes in the three Raman modes as a function of the unit-cell volume, which linearly decreases with x, for Ce$_{1-x}$Ca$_x$VO$_{4-0.5x}$ and Ce$_{1-x}$Bi$_x$VO$_4$.

TABLE 1
Grüneisen Parameters of the 847-cm^{-1}, 372-cm^{-1}, and 261-cm^{-1} Modes in $Ce_{1-x}Ca_xVO_{4-0.5x}$ and $Ce_{1-x}Bi_xVO_4$[a]

Mode (cm^{-1})	$Ce_{1-x}Ca_xVO_{4-0.5x}$	$Ce_{1-x}Bi_xVO_4$
847	0.58	0
372	−0.80	−0.80
261	−0.34	−1.84

[a] These parameters were determined from the changes in the modes' frequency with the unit-cell volume as shown in Fig. 4.

mode Grüneisen parameters, γ_{847}, γ_{372}, and γ_{210}, thus determined for $Ce_{1-x}Ca_xVO_{4-0.5x}$ and $Ce_{1-x}Bi_xVO_4$, are summarized in Table 1.

As expected, the Grüneisen parameters vary depending on the mode, the size and/or sign, and between $Ce_{1-x}Ca_xVO_{4-0.5x}$ and $Ce_{1-x}Bi_xVO_4$; this indicates that different lattice distortions are induced in the two cerium-based vanadates. Unfortunately, no mode Grüneisen parameters are available for the cerium and related vanadates, making it impossible to compare with the present results. Mode Grüneisen parameters are mostly determined from changes in Raman modes' frequency with pressure, since Eq. [1] reduces to $\gamma_i = B_T/\omega_i(d\omega_i/dP)$, with the isothermal bulk modulus $B_T = -V(dP/dV)_T$ (18, 20). In this situation, we measure the Raman spectra of $Ce_{1-x}Ca_xVO_{4-0.5x}$ and $Ce_{1-x}Bi_xVO_4$ as well as $CeVO_4$ with pressure to obtain the mode Grüneisen parameters. This will shed light on the lattice distortions when pressure is applied or when aliovalent or isovalent cations are substituted for Ce in $CeVO_4$. By that time, we cannot go into detail on the mode Grüneisen parameters in the cerium and related vanadates. Nevertheless, it is of interest that the Grüneisen parameters are different depending on the mode, the size and/or sign, and between $Ce_{1-x}Ca_xVO_{4-0.5x}$ and $Ce_{1-x}Bi_xVO_4$, where aliovalent or isovalent cations are substituted for their formation.

CONCLUSION

The Raman spectra of $Ce_{1-x}Ca_xVO_{4-0.5x}$ ($0 \leq x \leq 0.41$) and $Ce_{1-x}Bi_xVO_4$ ($0 \leq x \leq 0.68$), are presented as a function of x for comparison with each other. A remarkable spectral feature was found: the three broa features appeared in the Raman spectra of $Ce_{1-x}Ca_xVO_{4-0.5x}$, whereas they were not detected in $Ce_{1-x}Bi_xVO_4$. The appearance of the broad features could be attributed to the charge transfer effect when aliovalent Ca^{2+} was substituted to form $Ce_{1-x}Ca_xVO_{4-0.5x}$. Also, we could estimate the mode Grüneisen parameters from the changes in the modes' frequency with unit-cell volume for $Ce_{1-x}Ca_xVO_{4-0.5x}$ and $Ce_{1-x}Bi_xVO_4$ for the first time. The Grüneisen parameters vary depending on the mode, the magnitude and/or sign, and between $Ce_{1-x}Ca_xVO_{4-0.5x}$ and $Ce_{1-x}Bi_xVO_4$. This implies that different lattice distortions are induced when aliovalent or isovalent cations with similar/different ionic radii are substituted for Ce in $CeVO_4$ and are responsible for the different lattice parameter/distinctive spectral changes between $Ce_{1-x}Ca_xVO_{4-0.5x}$ and $Ce_{1-x}Bi_xVO_4$.

REFERENCES

1. A. Watanabe, *J. Solid State Chem.* **153,** 174 (2000).
2. H. Fuess and A. Kallel, *J. Solid State Chem.* **5,** 11 (1972).
3. B. C. Chakoumakous, M. M. Abraham, and L. A. Boather, *J. Solid State Chem.* **109,** 197 (1994).
4. M. Yoshimura and T. Sata, *Bull. Chem. Soc. Jpn.* **42,** 3195 (1969).
5. R. D. Shannon, *Acta Crystallogr. A* **32,** 751 (1976).
6. R. F. Reidy and K. E. Swider, *J. Am. Ceram. Soc.* **78,** 1121 (1995).
7. U. Opara Krasovec, B. Orel, A. Surca, N. Bukovec, and R. Reisfeld, *Solid State Ionics* **118,** 195 (1999).
8. E. J. Baran and P. J. Aymonino, *Z. Anorg. Allg. Chemie.* **383,** 226 (1971).
9. E. J. Baran, M. E. Escobar, L. L. Fournier, and R. R. Filqueira, *Z. Anorg. Allg. Chemie.* **472,** 193 (1981).
10. M. Kakihana, M. Osada, M. Käll, L. Börjesson, H. Mazaki, H. Yasuoka, M. Yashima, and M. Yoshimura, *Phys. Rev. B* **53,** 11796 (1996).
11. H. B. Radousky, K. F. McCarty, J. L. Peng, and R. N. Shelton, *Phys. Rev. B* **39,** 12383 (1989).
12. H. J. Rosen, R. M. Macfarlane, E. M. Engler, V. Y. Lee, and R. D. Jacowitz, *Phys. Rev. B* **38,** 2460 (1988).
13. X. H. Chen, K. Q. Ruan, G. G. Qian, S. Y. Li, L. Z. Cao, J. Zou, and C. Y. Xu, *Phys. Rev. B* **58,** 5868 (1988).
14. Xingjiang Zhou, M. Cardona, C. W. Chu, Q. M. Lin, S. M. Loureiro, and M. Marezio, *Phys. Rev. B* **54,** 6137 (1996).
15. D. Palles, N. Poulakis, E. Liarokapis, K. Conder, E. Kaldas, and K. A. Müller, *Phys. Rev. B* **54,** 6721 (1996).
16. M. Ocana, V. Fornes, J. V. Grarcia-Ramos, and C. J. Serna, *J. Solid State Chem.* **75,** 364 (1998).
17. S. P. S. Porto, P. A. Fleury, and T. C. Damen, *Phys. Rev.* **154,** 522 (1967).
18. T. Hirata, *Phys. Status Solidi B* **209,** 17 (1998).
19. R. Rubbin, *J. Phys. Chem. Solids* **52,** 941 (1991).
20. Y. Guyot, L. Grosvalet, B. Champagnon, E. Reny, C. Cros, and M. Pouchard, *Phys. Rev. B* **60,** 14507 (1997).